Emergence of nontrivial magnetic excitations in a spin-liquid state of kagomé volborthite

Daiki Watanabe[a,b], Kaori Sugii[a], Masaaki Shimozawa[a], Yoshitaka Suzuki[a], Takeshi Yajima[a], Hajime Ishikawa[a], Zenji Hiroi[a], Takasada Shibauchi[c], Yuji Matsuda[b], and Minoru Yamashita[a,1]

[a]Institute for Solid State Physics, University of Tokyo, Chiba 277-8581, Japan; [b]Department of Physics, Kyoto University, Kyoto 606-8502, Japan; and [c]Department of Advanced Materials Science, University of Tokyo, Chiba 277-8561, Japan

Edited by Gabriel Aeppli, ETH Zurich, Villigen PSI, Switzerland, and approved June 17, 2016 (received for review December 9, 2015)

When quantum fluctuations destroy underlying long-range ordered states, novel quantum states emerge. Spin-liquid (SL) states of frustrated quantum antiferromagnets, in which highly correlated spins fluctuate down to very low temperatures, are prominent examples of such quantum states. SL states often exhibit exotic physical properties, but the precise nature of the elementary excitations behind such phenomena remains entirely elusive. Here, we use thermal Hall measurements that can capture the unexplored property of the elementary excitations in SL states, and report the observation of anomalous excitations that may unveil the unique features of the SL state. Our principal finding is a negative thermal Hall conductivity κ_{xy} which the charge-neutral spin excitations in a gapless SL state of the 2D kagomé insulator volborthite $Cu_3V_2O_7(OH)_2\cdot 2H_2O$ exhibit, in much the same way in which charged electrons show the conventional electric Hall effect. We find that κ_{xy} is absent in the high-temperature paramagnetic state and develops upon entering the SL state in accordance with the growth of the short-range spin correlations, demonstrating that κ_{xy} is a key signature of the elementary excitation formed in the SL state. These results suggest the emergence of nontrivial elementary excitations in the gapless SL state which feel the presence of fictitious magnetic flux, whose effective Lorentz force is found to be less than 1/100 of the force experienced by free electrons.

spin liquid | frustrated magnetism | thermal transport

Spin liquids (SLs) are novel states which can occur in a magnetic system when the underlying magnetic order gives way to quantum fluctuations (1). In such states the constituent spins are highly correlated but continue to fluctuate strongly down to temperatures much lower than the spin-interaction energy scale, J. Novel notions such as emergent gauge fields, topological order, and fractionalized excitations have been associated with collective phenomena in SLs. In particular, both experiments (2–5) and theories (6–11) suggest that SL states display many unusual properties. It has been reported, for instance, that low-energy spin excitations in organic insulators with a triangular lattice structure behave like mobile carriers in a paramagnetic metal with a Fermi surface (2, 3), in contrast with the charge degree of freedom which is gapped. A description in terms of an SL state with fractionalized spin excitations was incorporated to account for the excitation continuum signal detected in a kagomé antiferromagnet (4). A magnetization transport measurement has shown that a pyrochlore frustrated magnet exhibits the characteristics of a supercooled SL state (5). Exotic quasi-particles such as spinons (6–8), visons (9, 10), and photons (11) have been predicted theoretically. Despite these intensive activities, the precise characters of the elementary excitations in SL states remain, from an experimental point of view, to be pinned down.

In conducting systems, it is the charge-transport properties that act as the window through which we accumulate information that are essential in unraveling the physics of novel electronic states such as the quantum Hall states and other non-Fermi liquids. Likewise, in insulating quantum magnets, thermal-transport measurements have been proven to be a powerful probe in unveiling the ground state and quasi-particle excitations (2, 12–16). Recently, theoretical works have suggested that thermal Hall measurements provide new insights into the nature of exotic excitations in magnetic insulators (17–20). In conducting systems, the electrical Hall (σ_{xy}) and thermal Hall (κ_{xy}) conductivities are related by the Wiedemann–Franz law $\kappa_{xy}/T = L\sigma_{xy}$ (21), where L is the Lorentz number. In magnetic insulators, in contrast, there are no charged currents, and thus a magnetic field cannot exert a Lorentz force. Nevertheless, the thermal Hall effect has been predicted to occur in both ordered (17, 18) and disordered magnets (17, 19, 20) as a result of the intrinsic Berry phase curvature and an emergent gauge field, respectively. Indeed, a finite κ_{xy} was reported in the ferromagnetic ordered state of magnetic insulators (12, 13). Very recently, its observation was also reported in the disordered states of the spin–ice compound $Tb_2Ti_2O_7$ (14) and the ferromagnetic kagomé Cu(1,3-bdc) (15). We note, however, that in the former study, a finite κ_{xy} was observed in the paramagnetic phase far above the temperature corresponding to J ($T \gg J/k_B \sim 1$ K) (22). Meanwhile, in the latter experiment there is no SL phase owing to the absence of geometrical frustration. In yet another study, thermal Hall measurements were performed in the SL state of triangular organic compound $EtMe_3Sb[Pd(dmit)_2]_2$, but no discernible κ_{xy} signal was observed (2). Thus, the experimental verification of thermal Hall conductivity in SL states remains a subject of vital importance.

Results

Heat Capacity and Magnetic Susceptibility Measurements. Volborthite, $Cu_3V_2O_7(OH)_2\cdot 2H_2O$, is a magnetic insulator in which Cu^{2+} ions form a 2D distorted kagomé structure with inequivalent exchange

Significance

The Hall effect is due to the nature of the charge carriers in a conductor, which experience the Lorentz force in the presence of magnetic field. In antiferromagnetic insulators with geometrical frustrations, charge carries are absent, but the spin degrees of freedom form disordered liquid-like states with unusual excitations that can carry heat. Here, we report the observation of the thermal version of the Hall effect in a spin-liquid state of a quantum magnet with frustrated two-dimensional kagomé structure. Our finding implies the emergence of nontrivial excitations in a spin-liquid state that experience the fictitious Lorentz force, possibly related to the geometrical phase of the quantum-mechanical wave function in many-body systems.

Author contributions: M.Y. designed research; D.W., K.S., M.S., Y.S., T.Y., H.I., Z.H., and M.Y. performed research; T.Y., H.I., and Z.H. performed synthesis and characterization of single crystals; D.W., K.S., M.S., Y.S., H.I., T.S., Y.M., and M.Y. analyzed data; and T.S., Y.M., and M.Y. wrote the paper.

The authors declare no conflict of interest.

This article is a PNAS Direct Submission.

[1]To whom correspondence should be addressed. Email: my@issp.u-tokyo.ac.jp.

This article contains supporting information online at www.pnas.org/lookup/suppl/doi:10.1073/pnas.1524076113/-/DCSupplemental.

PHYSICS

interactions (23–26) (Fig. 1, *Inset*). The temperature dependence of the magnetic susceptibility χ shows a behavior that is typical of 2D frustrated spin systems (Fig. 1). Below $T^* \sim 60$ K, $\chi(T)$ begins to deviate from the paramagnetic Curie–Weiss behavior (24, 27, 28), implying that the spin correlations grow gradually when the temperature energy scale $k_B T^*$ becomes comparable to the effective spin-interaction energy J_{eff}. A peak of $\chi(T)$ at $T_p \sim 18$ K suggests that spins are highly correlated at lower temperatures. Recently, based on the observation of an extremely wide one-third magnetization plateau (26), effective spin Hamiltonians featuring coupled frustrated chains (27) and coupled trimers (28) were proposed. In the latter framework, the system can be viewed as a frustrated triangular lattice with competing antiferromagnetic and ferromagnetic interactions with exchange couplings whose energy scales are not far from $k_B T^*$. In either model, the combination of strong geometrical frustration with enhanced quantum fluctuations for $S = 1/2$ suppresses the magnetic ordering down to $T_N \sim 1$ K (~ 2 K) at zero field (15 T) (24, 25), which infers the presence of an SL state in a wide temperature range $T_N < T < T^* \sim J_{\rm eff}/k_B$. Clearly the χ above T_N extrapolated to $T = 0$ remains finite, suggesting the gapless nature of the spin excitations in the SL state. Strong evidence supporting the presence of the gapless excitations comes from the specific heat measurements at low temperatures (Fig. 1), which show a large linear temperature-dependent contribution, $C/T(T \to 0) \sim 50$ mJ K^{-2} mol$-$Cu^{-1}.

Longitudinal and Transverse Thermal Conductivities. Fig. 2 *A* and *B* shows the temperature dependences of the longitudinal thermal conductivity, κ_{xx}/T, of sample 1 (2) in zero field and in a magnetic field of 15 T (H⊥2D plane). The thermal conductivity was measured along the *b* axis in measurements of sample 1. In sample 2, the thermal conductivities along the *a* axis ($\kappa_{xx,a}$) and that along the *b* axis ($\kappa_{xx,b}$) were measured (Fig. 2*B*). In all measurements, we find that the magnetic field of 15 T suppresses κ_{xx}/T below $\sim T_{\rm p}$. This suppression arises from the field effect on the thermal conduction of spin excitations $\kappa_{xx}^{\rm spin}$ and the resonance scattering effect on the thermal conduction of phonons κ_{xx}^{ph}. In the present system, heat is transferred by spin excitations and phonons: $\kappa_{xx} = \kappa_{xx}^{\rm spin} + \kappa_{xx}^{\rm ph}$. The field dependence of $\kappa_{xx}^{\rm ph}$ is determined by the spin–phonon scattering and the resonant scattering (29). The former contains elastic and inelastic processes. The elastic scattering process is suppressed by the alignment of spins with the magnetic field. The inelastic scattering is directly related to the quantum dynamics of spin, which is also suppressed with field by the formation of the Zeeman gap. Therefore, an application of magnetic fields leads to a suppression of the spin–phonon scattering (an enhancement of $\kappa_{xx}^{\rm ph}$), which is observed at higher temperatures where $\kappa_{xx}^{\rm ph}$ is dominant ($T > 20$ K, Fig. S1). The latter is due to a resonance between the Zeeman gap $g\mu_B H$ and the phonon, blocking the energy transfer of phonons whose energy $\hbar\omega \sim g\mu_B H$, where g is the g factor and μ_B is the Bohr magneton (29). The resonance scattering causes a suppression peak when the Zeeman energy is equal to the peak of the Debye distribution function ($\sim 4k_B T$). Also, a normalized suppression effect is often observed when $[\kappa_{xx}(H) - \kappa_{xx}(0)]/\kappa_{xx}(0)$ is plotted as a function of $g\mu_B H/k_B T$ (*SI Text*). As shown in Fig. 2 *C* and *D*, a suppression peak is observed at 2.6 K and at ~7 T ($g\mu_B H/k_B T \sim 4$), showing the resonance coupling effect on κ_{xx}^{ph}. However, this suppression peak is taken over by another suppression effect at 15 T. At higher temperatures, this additional suppression, which can be attributed to the field effect on $\kappa_{xx}^{\rm spin}$, becomes dominant and the resonant coupling peak is no longer discernible at 3.5 ~ 5.0 K. Moreover, we find that the field dependences of κ_{xx} at high fields cannot be scaled by $g\mu_B H/k_B T$ due to the additional suppression effect. Therefore, from the field suppression effect on κ_{xx}^{spin} observed at high fields, we can conclude that the spins contribute to the thermal transport in volborthite.

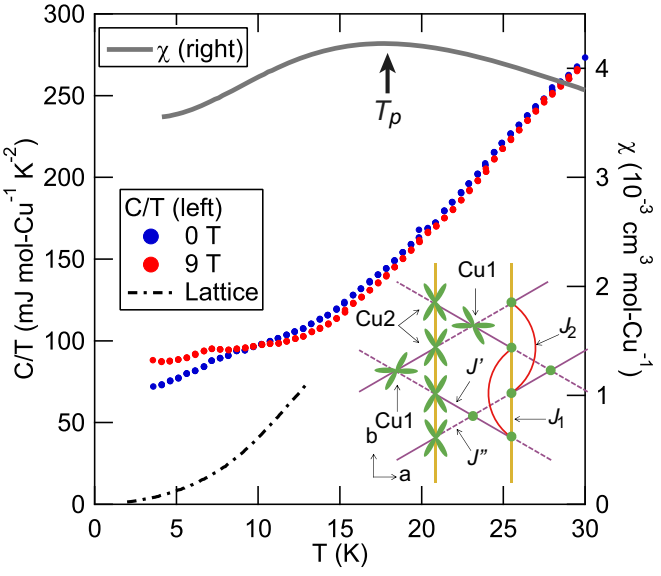

Fig. 1. Temperature dependence of the heat capacity divided by temperature C/T (closed circles, left axis) and the magnetic susceptibility χ (gray line, right axis) of a single crystal of volborthite. The peak temperature of the magnetic susceptibility is marked as T_p. Dashed line is the lattice heat capacity taken from ref. 36. At ~7 K, C/T shows a kink in zero field, which is pronounced in the magnetic field of 9 T. However, no signature of a magnetic transition has been observed in NMR and magnetic susceptibility measurements at this temperature. Therefore, the kink may be related to a lattice anomaly, although no discernible anomaly is observed in the thermal conductivity. (*Inset*) Arrangement of Cu ions in the *ab* plane. J_1 and J_2 represent the nearest-neighbor and next-nearest-neighbor interactions in the Cu2 spin chains, respectively. J' and J'' represent the nearest-neighbor interactions between Cu1 and Cu2 spins.

The thermal conductivity of spin excitations can be expressed as $\kappa_{xx}^{\rm spin} \sim C_{\rm spin} v_{\rm spin} \ell_{\rm spin}$, where $C_{\rm spin}$ is the heat capacity, $v_{\rm spin}$ is the velocity, and $\ell_{\rm spin}$ is the mean-free path of the elementary spin excitations. Because the magnetic field enhances $\ell_{\rm spin}$ by aligning spins and $C_{\rm spin}$ shows only a weak field dependence around 8 K (Fig. 1), the field suppression of $\kappa_{xx}^{\rm spin}$ is dominated by the suppression of $v_{\rm spin}$. Similar results have been reported in spin–chain compounds (16) where the velocity of elementary excitations is suppressed by fields. The lower limit of $\ell_{\rm spin}$ is simply estimated by assuming that $\Delta\kappa = \kappa_{xx}(H = 0) - \kappa_{xx}(H = 15\ T)$ gives a lower limit of $\kappa_{xx}^{\rm spin}$. From the assumption of a linear energy dispersion, the velocity is obtained as $v_{\rm spin} \sim J_{eff} a/\hbar \sim 2.3 \times 10^3$ m/s, where $J_{eff} \sim 60$ K and $a \sim 2.9$ Å is the mean distance between the nearest Cu ions. From $C_{\rm spin}/T \sim 50$ mJ K^{-2} mol$-$Cu^{-1} and $\Delta\kappa/T \sim 0.03$ (0.09) W K$^{-2}\cdot$m^{-1} for sample 1 (2) at ~8 K, we find the lower limit of $\ell_{\rm spin} \sim 23$ nm (69 nm) $\sim 80\ a$ (240 a), indicating that the elementary excitations are highly mobile.

To gain insight into the spin Hamiltonian realized in volborthite, we investigated the anisotropy of the thermal conduction. As shown in Fig. 2*B*, we find that $\kappa_{xx,a} \sim \kappa_{xx,b}$ within the accuracy of the absolute value of κ_{xx} (up to ~30% due to the uncertainty in estimating the geometrical factor). Also, $\kappa_{xx,a}$ and $\kappa_{xx,b}$ show the similar field dependence (Fig. 2 *C* and *D*), although the field suppression effect on $\kappa_{xx,b}$ is slightly larger (~5% of the zero-field value) than that on $\kappa_{xx,a}$. These results would imply a small anisotropy in the spin Hamiltonian, supporting the coupled trimer model (28) rather than the coupled chain model (27). Below T_N, $\kappa_{xx,a}$ shows a larger enhancement than that of $\kappa_{xx,b}$, implying an anisotropic spin state in the ordered phase.

Fig. 3*A* depicts the transverse thermal response of sample 1 along the *y* axis, $\Delta T_y \equiv T_{L1} - T_{L2}$, at 8.3 K when the magnetic

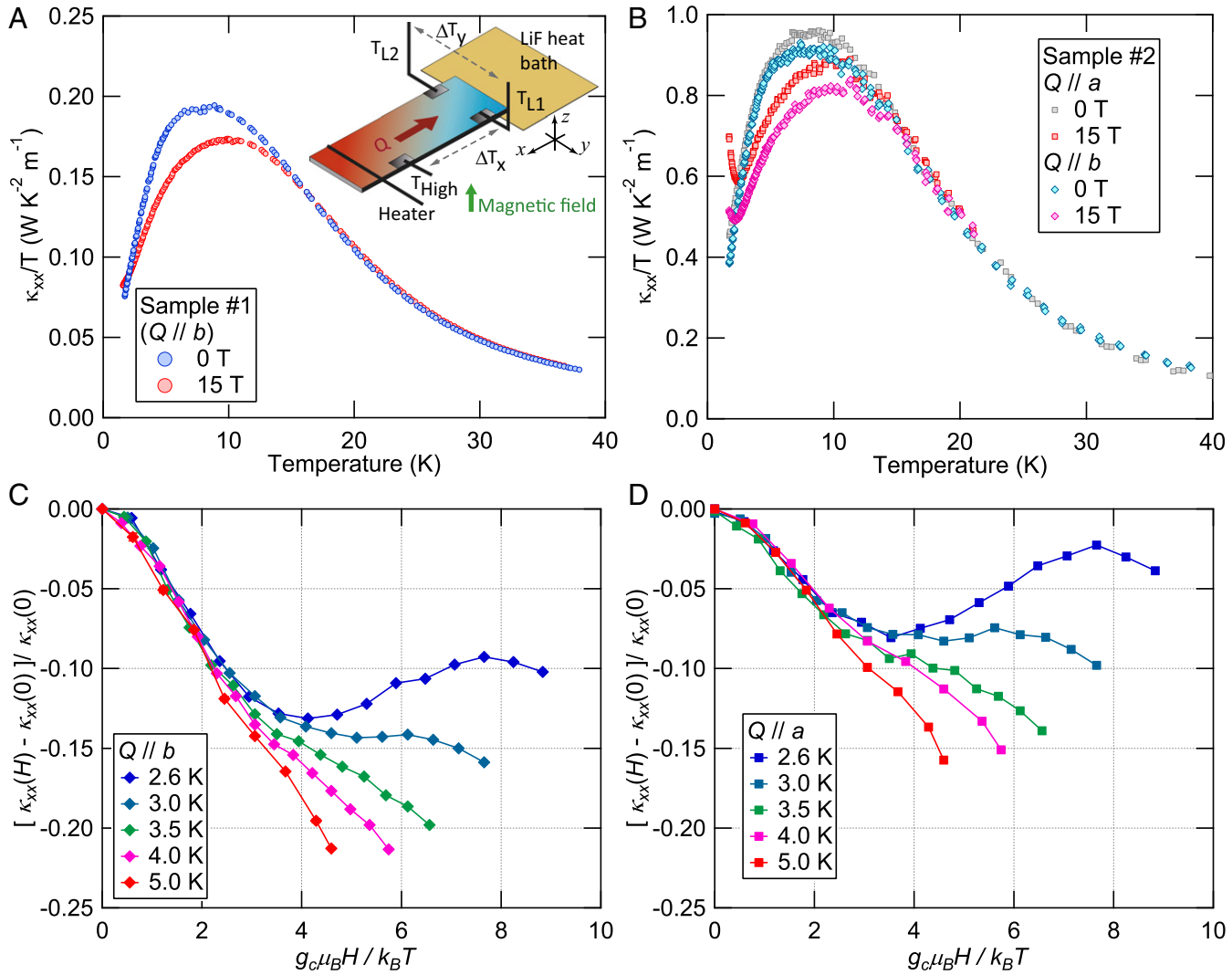

Fig. 2. Longitudinal thermal conductivities of volborthite. (*A*) Temperature dependence of κ_{xx}/T of sample 1 at 0 T (blue) and 15 T (red). The heat current (*Q*) was applied along the *b* axis of the sample. (*Inset*) Our experimental setup. Three thermometers (T_{High}, T_{L1}, T_{L2}) were attached to the sample. A heater was attached at one end of the sample to produce the thermal gradient along the *x* axis. The magnetic field was applied along the *z* axis. The temperature differences ΔT_x and ΔT_y were defined as $T_{High} - T_{L1}$ and $T_{L1} - T_{L2}$, respectively. (*B*) Temperature dependence of κ_{xx}/T of sample 2 where the thermal conductivities both along the *a* axis ($\kappa_{xx,a}$) and the *b* axis ($\kappa_{xx,b}$) were measured. (*C* and *D*) The field dependence of $\kappa_{xx,b}$ (*C*) and $\kappa_{xx,a}$ (*D*) plotted as a function of $g_c\mu_B H/k_B T$ [$g_c = 2.28$ (26)]. The error bars are smaller than the symbol size for all figures, except the error in the absolute value of κ_{xx} due to the uncertainty in estimating the geometrical factor.

field is applied perpendicular to the 2D plane ($\boldsymbol{H} \parallel z$) in the presence of the thermal current along the *x* axis. The longitudinal response due to misalignment of the contacts is canceled by reversing the magnetic field. As shown in Fig. 3*B*, the antisymmetrized thermal response with respect to the field direction, $\Delta T_y^{\mathrm{Asym}}(H) \equiv [\Delta T_y(+H) - \Delta T_y(-H)]/2$, is clearly resolved, establishing a finite thermal Hall effect. Special care was taken to detect the intrinsic thermal Hall signal from the sample (*SI Text* and Fig. S2). Fig. 4 depicts the temperature dependence of $-\kappa_{xy}/TB$ at the field of 15 T. Finite thermal Hall signal appears at $T \lesssim T^* \sim 60$ K. The sign of κ_{xy} is negative, i.e., electron-like. As the temperature is lowered, $-\kappa_{xy}/TB$ first develops gradually and then increases steeply below 30 K. After reaching a maximum at around 15 K, $-\kappa_{xy}/TB$ decreases rapidly and changes sign slightly above T_N. It should be stressed that no discernible thermal Hall signal is observed in the paramagnetic state at $T \gtrsim T^* \sim 60$ K. Moreover, $-\kappa_{xy}/TB$ or $-\kappa_{xy}$ exhibits a peak at $\sim T_p$ where χ becomes maximum due to the development of the spin–spin correlation length (Fig. 4, *Inset*). These results lead us to conclude that the observed thermal Hall effect in volborthite arises from the magnetic excitations in the SL state, not from phonons (*SI Text*).

Discussion

We first discuss the relation between the observed thermal Hall effect and the strength of the Dzyloshinsky–Moriya (DM) interaction induced by the spin–orbit coupling. In the case of the magnon Hall effect, the thermal Hall conductivity is well understood in terms of the Berry curvature formed by the DM interaction (12, 13, 17, 18). The DM interaction has also been pointed to play an essential role for the thermal Hall effect in disordered magnets (14, 15, 17, 19, 20). In volborthite, because of the low symmetry of the distorted kagomé structure, there is nonzero DM interaction. Although the detail direction and the magnitude of the DM interaction have not been known, the magnitude of the DM interaction (D) can be estimated as $D/J \sim 0.1$ from the g factors [$g_c = 2.28$, and $g_{ab} = 2.18$ (26)]. We thus find that D/J is about 2 orders of magnitude larger than the upper limit of the Hall angle $(\kappa_{xy}/T)/(\kappa_{xx}^{\mathrm{spin}}/T) \sim -1 \times 10^{-3}$

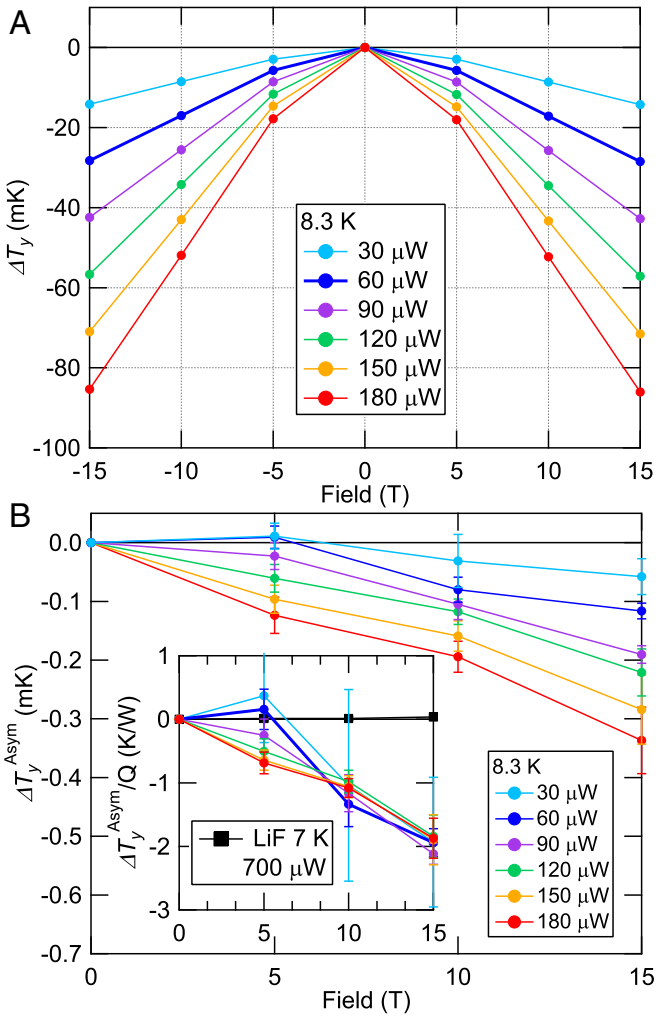

Fig. 3. Transverse temperature differences as a function of the fields and the heater powers. (*A*) The transverse temperature difference $\Delta T_y(H) \equiv T_{L1}(H) - T_{L2}(H)$ of sample 1 at 8.3 K. For clarity, data are vertically offset so that $\Delta T_y(H=0)=0$. The symmetric field dependence of κ_{xx} is included due to misalignment of the contacts. The error bars are smaller than the symbol size. (*B*) The antisymmetrized transverse temperature difference, $\Delta T_y^{\mathrm{Asym}}(H) \equiv (\Delta T_y(+H) - \Delta T_y(-H))/2$, of the same data. (*Inset*) The data normalized by the heater power, together with the data at 7 K of a LiF crystal used as the heat bath (black squares). The error bars correspond to 1 SD.

obtained by $\kappa_{xx}^{\mathrm{spin}}/T > \Delta\kappa/T \sim 0.03$ W K^{-2} · m^{-1} and $\kappa_{xy} \sim -3\times 10^{-4}$ W K^{-1} · m^{-1} at 8 K and 15 T. In the ferromagnetic kagomé Cu(1,3-bdc), a similar size of the DM interaction $D/J \sim 0.15$ is reported (15), whereas the thermal Hall signal is 1–2 orders of magnitude larger than that of volborthite, implying a different origin of the thermal Hall signal in frustrated antiferromagnets and that in ferromagnets. We note that a large Ising anisotropy of ~10 is reported in $Tb_2Ti_2O_7$ (30). This large anisotropy (thus a strong spin–orbit interaction) may be related to the large thermal Hall signal observed in $Tb_2Ti_2O_7$ (14).

According to Katsura et al. (17), deconfined spin excitations couple to an emergent gauge field. Through the coupling between the vector potential and the gauge flux, the external magnetic field can exert a Lorentz force on spin excitations, which gives rise to a finite Hall effect, just as in the case of charged particles. Although applying this theory to the present system simply should be scrutinized, it is tempting to compare the Lorentz force acting on the spin excitations in volborthite with that acting on the free electrons. Assuming the Wiedemann–Franz law for the spin excitation (*SI Text*), we find that the ratio of the Lorentz force acting on the spin excitations and that on electrons is estimated to be $|(eB)_{\mathrm{spin}}/(eB)_e| \sim 8\times 10^{-3}$ at most. This implies that the coupling between the applied magnetic field and the gauge flux in an SL state is very small (31). Such a small coupling may be a reason for the absence of the quantum oscillations in an SL state of $EtMe_3Sb[Pd(dmit)_2]_2$ (3). We also note that this value is ~4 orders of magnitude smaller than the estimate reported in the paramagnetic state of $Tb_2Ti_2O_7$ (14).

At low temperatures below T_p where the spin–spin correlation grows rapidly, κ_{xy}/T shows a rapid reduction and changes the sign slightly above T_N. This suppression of $\kappa_{xy}/T \sim (C_{\mathrm{spin}}/T)(\ell_{\mathrm{spin}})^2(eB)_{\mathrm{spin}}/m_{\mathrm{spin}}$ is unusual, because C_{spin}/T and ℓ_{spin} do not show large temperature dependencies in this temperature range. There are several possible origins for this suppression. The suppression of $(eB)_{\mathrm{spin}}$ may appear as a result of an instability of the fictitious gauge flux when the system approaches the ordered phase (31). Another possibility is the emergence of an additional spin excitation with the opposite sign of $(eB)_{\mathrm{spin}}$. A kagomé structure gives rise to two types of hopping loops, triangular and hexagonal (17). The strong spin–spin correlations at low temperatures can generate spin excitations of the long hexagonal loop, which may induce a different sign of κ_{xy}. Further experimental studies on other frustrated SL systems may be important to clarify these nontrivial issues.

Materials and Methods

The single crystals of volborthite used in this study were prepared by hydrothermal synthesis. Typical sample size is ~1 mm ×0.5 mm×0.05 mm. The crystals have an arrowhead-like shape with one twin boundary in the middle (26). All single crystals used in the thermal conductivity measurements were detwinned by cutting in half at the middle. The thermal conductivity and the thermal Hall conductivity were measured by the standard steady-state method in a variable temperature insert for 1.7 K to 80 K. An illustration of the setup is shown in the Fig. 2*A* (*Inset*). In measurements of sample 1, a heat current (Q) was applied along the b axis of the sample. In sample 2, we measured the longitudinal thermal conductivities along both the a and the b axes (Fig. 2*B*). The magnetic field, $\mu_0 H \leq 15$ T, was applied perpendicular to the kagomé plane. We attached three Cernox thermometers (CX1050) and one heater on the samples. The configuration of the three thermometers (T_{High}, T_{L1}, T_{L2}) is shown in Fig. 2*A* (*Inset*). These thermometers were carefully calibrated in fields. We confirmed that all three thermometers show

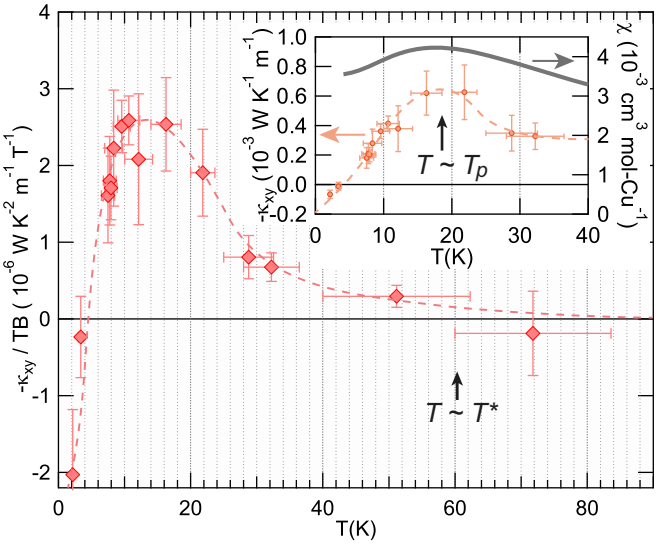

Fig. 4. Temperature dependence of $-\kappa_{xy}/TB$ at 15 T (sample 1). (*Inset*) $-\kappa_{xy}$ at 15 T (*Left*) and χ (*Right*). The dashed lines are guides to the eye. The error bars correspond to 1 SD.

the identical magnetoresistance, which matches that of the previous work (32) within our resolution. There is a large sample dependence in the magnitude of the longitudinal thermal conductivity of volborthite. The thermal Hall measurements were mainly done in crystals with low thermal conduction because samples of lower κ_{xx} show larger ΔT_y.

The longitudinal thermal conductivity, κ_{xx}, and the thermal Hall conductivity, κ_{xy}, are obtained by

$$\frac{1}{wt}\begin{pmatrix} Q \\ 0 \end{pmatrix} = \begin{pmatrix} \kappa_{xx} & \kappa_{xy} \\ -\kappa_{xy} & \kappa_{xx} \end{pmatrix} \begin{pmatrix} (T_{High} - T_{L1})/L \\ (T_{L1} - T_{L2})/w \end{pmatrix} = \begin{pmatrix} \kappa_{xx} & \kappa_{xy} \\ -\kappa_{xy} & \kappa_{xx} \end{pmatrix} \begin{pmatrix} \Delta T_x/L \\ \Delta T_y/w \end{pmatrix},$$

where $\Delta T_x \equiv T_{High} - T_{L1}$, $\Delta T_y \equiv T_{L1} - T_{L2}$, t is the thickness of the sample, and L (w) is the distance between the thermal contacts for T_{High} and T_{L1} (T_{L1} and T_{L2}).

In nonmagnetic insulators, the thermal conductivity is provided by phonons ($\kappa_{xx} = \kappa_{xx}^{ph}$) and there is no thermal Hall conductivity $\kappa_{xy} = 0$ because the thermal Hall effects of phonons require couplings between phonons and spins as scatters of phonons (*SI Text*). The temperature dependence and the orders of magnitude of κ_{xx}^{ph} depend on materials. Generally, κ_{xx}^{ph} shows a peak at 10–30 K due to a cross-over of the dominant relaxation process which is limited by the Umklapp processes or defects in high temperatures, but is limited by boundaries in low temperatures. In an isotopically pure insulator LiF, the thermal conductivity is ~ 200 W K$^{-1}\cdot$m^{-1} at 50 K and has a peak of $1{,}000 \sim 10{,}000$ W K$^{-1}\cdot$m^{-1} at $\sim$10 K (33). The thermal conductivity of the ordered insulator MnF_2 (34) and the ordered metal chromium (35) also show a similar temperature dependence with a peak of ~ 600 W K$^{-1}\cdot$m^{-1} at $\sim$15 K and ~ 500 W K$^{-1}\cdot$m^{-1} at $\sim$25 K, respectively. This phonon peak is also observed in volborthite at $\sim$15 K (Fig. S3).

ACKNOWLEDGMENTS. We thank K. Behnia, H. Katsura, P. A. Lee, T. Momoi, O. I. Motrunich, N. Nagaosa, S. Onoda, T. Senthil, A. Shitade, H. Takatsu, and C. Varma for valuable discussions. This work was carried out under the Visiting Researcher's Program of the Institute for Solid State Physics, University of Tokyo. This research was funded by Yamada Science Foundation, Toray Science Foundation, and KAKENHI (Grants-in-Aid for Scientific Research) from Japan Society for the Promotion of Science and by a Grant-in-Aid for Scientific Research on Innovative Areas "Topological Materials Science" (KAKENHI Grant 15H05852).

1. Balents L (2010) Spin liquids in frustrated magnets. *Nature* 464(7286):199–208.
2. Yamashita M, et al. (2010) Highly mobile gapless excitations in a two-dimensional candidate quantum spin liquid. *Science* 328(5983):1246–1248.
3. Watanabe D, et al. (2012) Novel Pauli-paramagnetic quantum phase in a Mott insulator. *Nat Commun* 3:1090.
4. Han TH, et al. (2012) Fractionalized excitations in the spin-liquid state of a kagome-lattice antiferromagnet. *Nature* 492(7429):406–410.
5. Kassner ER, et al. (2015) Supercooled spin liquid state in the frustrated pyrochlore $Dy_2Ti_2O_7$. *Proc Natl Acad Sci USA* 112(28):8549–8554.
6. Motrunich OI (2005) Variational study of triangular lattice spin-1 /2 model with ring exchanges and spin liquid state in κ-$(ET)_2Cu_2(CN)_3$. *Phys Rev B* 72(4):045105.
7. Lee SS, Lee PA (2005) U(1) gauge theory of the Hubbard model: Spin liquid states and possible application to κ-(BEDT-TTF)2Cu2(CN)3. *Phys Rev Lett* 95(3):036403.
8. Mross DF, Senthil T (2011) Charge Friedel oscillations in a Mott insulator. *Phys Rev B* 84(4):R041102.
9. Read N, Sachdev S (1991) Large-N expansion for frustrated quantum antiferromagnets. *Phys Rev Lett* 66(13):1773–1776.
10. Senthil T, Fisher MP (2001) Fractionalization in the cuprates: Detecting the topological order. *Phys Rev Lett* 86(2):292–295.
11. Gingras MJ, McClarty PA (2014) Quantum spin ice: A search for gapless quantum spin liquids in pyrochlore magnets. *Rep Prog Phys* 77(5):056501.
12. Onose Y, et al. (2010) Observation of the magnon Hall effect. *Science* 329(5989):297–299.
13. Ideue T, et al. (2012) Effect of lattice geometry on magnon Hall effect in ferromagnetic insulators. *Phys Rev B* 85(13):134411.
14. Hirschberger M, Krizan JW, Cava RJ, Ong NP (2015) Frustrated magnetism. Large thermal Hall conductivity of neutral spin excitations in a frustrated quantum magnet. *Science* 348(6230):106–109.
15. Hirschberger M, Chisnell R, Lee YS, Ong NP (2015) Thermal Hall effect of spin excitations in a kagome magnet. *Phys Rev Lett* 115(10):106603.
16. Sologubenko AV, et al. (2007) Magnetothermal transport in the spin-1/2 chains of copper pyrazine dinitrate. *Phys Rev Lett* 98(10):107201.
17. Katsura H, Nagaosa N, Lee PA (2010) Theory of the thermal Hall effect in quantum magnets. *Phys Rev Lett* 104(6):066403.
18. Matsumoto R, Shindou R, Murakami S (2014) Thermal Hall effect of magnons in magnets with dipolar interaction. *Phys Rev B* 89(5):054420.
19. Romhányi J, Penc K, Ganesh R (2015) Hall effect of triplons in a dimerized quantum magnet. *Nat Commun* 6:6805.
20. Lee H, Han JH, Lee PA (2015) Thermal Hall effect of spins in a paramagnet. *Phys Rev B* 91(12):125413.
21. Zhang Y, et al. (2000) Determining the Wiedemann-Franz ratio from the thermal Hall conductivity: Application to Cu and $YBa_2Cu_3O_{6.95}$. *Phys Rev Lett* 84(10):2219–2222.
22. Takatsu H, et al. (2016) Quadrupole order in the frustrated pyrochlore $Tb_{2+x}Ti_{2-x}O_{7+y}$. *Phys Rev Lett* 116(21):217201.
23. Hiroi Z, et al. (2001) Spin-1/2 *Kagomé*–like lattice in volborthite $Cu_3V_2O_7(OH)_2\cdot 2H_2O$. *J Phys Soc Jpn* 70(11):3377–3384.
24. Yoshida H, et al. (2012) Orbital switching in a frustrated magnet. *Nat Commun* 3:860.
25. Yoshida M, et al. (2012) High-field phase diagram and spin structure of volborthite $Cu_3V_2O_7(OH)_2\cdot 2H_2O$. *J Phys Soc Jpn* 81(2):024703.
26. Ishikawa H, et al. (2015) One-third magnetization plateau with a preceding novel phase in volborthite. *Phys Rev Lett* 114(22):227202.
27. Janson O, Richter J, Sindzingre P, Rosner H (2010) Coupled frustrated quantum spin-1/2 chains with orbital order in volborthite $Cu_3V_2O_7(OH)_2\cdot 2H_2O$. *Phys Rev B* 82(10):104434.
28. Janson O, et al. (2015) Magnetic behavior of volborthite $Cu_3V_2O_7(OH)_2\cdot 2H_2O$ determined by coupled trimers rather than frustrated chains. arXiv:1509.07333.
29. Berman R (1976) *Resonant Scattering. Thermal Conduction in Solids* (Oxford Univ Press, Oxford), pp 91–99.
30. Cao H, et al. (2009) Ising versus *XY* anisotropy in frustrated $R_2Ti_2O_7$ compounds as "seen" by polarized neutrons. *Phys Rev Lett* 103(5):056402.
31. Motrunich OI (2006) Orbital magnetic field effects in spin liquid with spinon Fermi sea: Possible application to κ-$(ET)_2Cu_2(CN)_3$. *Phys Rev B* 73(15):155115.
32. Brandt BL, Liu DW, Rubin LG (1999) Low temperature thermometry in high magnetic fields. VII. Cernox sensors to 32 T. *Rev Sci Instrum* 70(1):104–110.
33. Thacher DP (1967) Effect of boundaries and isotopes on the thermal conductivity of LiF. *Phys Rev* 156(3):975–988.
34. Slack GA (1961) Thermal conductivity of CaF2, MnF2, CoF2, and ZnF2 crystals. *Phys Rev* 122(5):1451–1464.
35. Harper AFA, Kemp WRG, Klemens PG, Tainsh RJ, White GK (1957) The thermal and electrical conductivity of chromium at low temperatures. *Philos Mag* 2(17):577–583.
36. Yamashita S, et al. (2010) Thermodynamic properties of the kagomé lattice in volborthite. *J Phys Soc Jpn* 79(8):083710.
37. Sheard FW, Toombs GA (1973) Resonant phonon scattering in a coupled spin-phonon system. *Solid State Commun* 12(7):713–716.
38. Block JCF, Huntley DJ (1968) Phonon mean free paths from magneto-thermal-conductivity measurements. *Can J Phys* 46(20):2231–2240.
39. Fox GT, Wolfmeyer MW, Dillinger JR, Huber DL (1969) Thermal conductivity of rare-earth-doped CaF_2 in magnetic fields. *Phys Rev* 181(3):1308–1311.
40. Sun XF, Tsukada I, Suzuki T, Komiya S, Ando Y (2005) Large magnetothermal effect and spin-phonon coupling in a parent insulating cuprate $Pr_{1.3}La_{0.7}CuO_4$. *Phys Rev B* 72(10):104501.
41. Strohm C, Rikken GLJA, Wyder P (2005) Phenomenological evidence for the phonon Hall effect. *Phys Rev Lett* 95(15):155901.
42. Inyushkin AV, Taldenkov AN (2007) On the phonon Hall effect in a paramagnetic dielectric. *JETP Lett* 86(6):379–382.
43. Sheng L, Sheng DN, Ting CS (2006) Theory of the phonon Hall effect in paramagnetic dielectrics. *Phys Rev Lett* 96(15):155901.
44. Wang JS, Zhang L (2009) Phonon Hall thermal conductivity from the Green-Kubo formula. *Phys Rev B* 80(1):012301.
45. Zhang L, Ren J, Wang JS, Li B (2010) Topological nature of the phonon Hall effect. *Phys Rev Lett* 105(22):225901.
46. Qin T, Zhou J, Shi J (2012) Berry curvature and the phonon Hall effect. *Phys Rev B* 86(10):104305.
47. Mori M, Spencer-Smith A, Sushkov OP, Maekawa S (2014) Origin of the phonon Hall effect in rare-earth garnets. *Phys Rev Lett* 113(26):265901.
48. Araki K, Goto T, Nemoto Y, Yanagisawa T, Lüthi B (2008) Magneto-elastic properties of $Tb_3Ga_5O_{12}$ (TGG). *Eur Phys J B* 61(3):257–259.
49. Sytcheva A, et al. (2010) Acoustic Faraday effect in $Tb_3Ga_5O_{12}$. *Phys Rev B* 81(21):214415.
50. Slack GA, Oliver DW (1971) Thermal conductivity of garnets and phonon scattering by rare-earth ions. *Phys Rev B* 5(2):592–609.
51. Guillot M, Marchand A (1985) Step-like magnetisation curves in $Tb_3Ga_5O_{12}$. *J Phys C Solid State Phys* 18(18):3547–3550.